electronics

Article

Ultra-Wideband Graphene-Based Micro-Sized Circular Patch-Shaped Yagi-like MIMO Antenna for Terahertz Wireless Communication

Abdullah G. Alharbi [1] and Vishal Sorathiya [2,*]

[1] Department of Electrical Engineering, Jouf University, Sakaka 42421, Saudi Arabia; a.g.alharbi@ieee.org
[2] Department of Information and Communication Technology, Marwadi University, Rajkot 360003, India
* Correspondence: vishal.sorathiya@marwadieducation.edu.in; Tel.: +91-9033-3160-57

Abstract: In this work, an ultra-wideband graphene-based micro-sized circular patch-shaped Yagi-like MIMO antenna was investigated over 1–30 THz of the frequency spectrum. The proposed antenna structure was designed over a polyimide substrate with 620 × 800 μm^2. This antenna was radiated over three bands over 1–30 THz. The maximum bandwidth achieved 10.96 THz, with −26 dB of the return loss isolation. These three bands were also mathematically analyzed using various MIMO antenna parameters to match the MIMO antenna criteria. This antenna provided all the accepted results as per the limits set by these antenna parameters. The effect of the different port excitation on the change of directivity of the overall structure is also reported. The MIMO antenna parameters such as TARC (Total Active Reflection Coefficient), ECC (Envelope Correlation Coefficient), MEG (Mean Effective Gain), CCL (Channel Capacity Loss), and DG (Directivity Gain) were investigated for the proposed structure. These values were also identified to check the compatibility and challenges associated with short-distance communication. The suggested THz MIMO antenna provides the operating bands of 1–10 THz and 15–30 THz, with good isolation values. An average of 7 dB gain was observed in the 2 × 2 antenna structure. The newly developed MIMO antenna in the THz frequency range may be used for high-speed short-distance and terahertz communications.

Keywords: terahertz; MIMO; antenna; graphene; wireless

Citation: Alharbi, A.G.; Sorathiya, V. Ultra-Wideband Graphene-Based Micro-Sized Circular Patch-Shaped Yagi-like MIMO Antenna for Terahertz Wireless Communication. *Electronics* **2022**, *11*, 1305. https://doi.org/10.3390/electronics11091305

Academic Editors: Amjad Iqbal, Issa Tamer Elfergani, Ismail Ben Mabrouk and Kiat Seng Yeo

Received: 18 March 2022
Accepted: 17 April 2022
Published: 20 April 2022

1. Introduction

Wireless communication technology has seen a significant shift in the last several decades due to the increasing need for higher data rates in the current trend of wireless communication [1]. Several new application possibilities have been created as a result of the fantastic research breakthroughs in mobile communication systems (3G to 5G), which have enabled increased data connection [2,3]. As a standard defined by the IEEE, with possible operating bands of 0.3–10 THz frequency range, Terahertz wireless communications (TeraCom, Stockholm, Sweden) may be the future wireless technology to fulfil the requirements of Tbps data rate and enormous channel capacity [4]. Scientists are researching terahertz communication at shorter wavelengths to take advantage of the greater bandwidth that can be unlocked and used for future large-scale civic and commercial applications. However, THz communications have both exciting potential and critical difficulties, such as significant propagation route loss and a limited communication distance, which must be considered. We must not forget the fact that the characteristics of the THz antenna have a direct influence on the performance of THz systems. Antennas for transmitting and sensing THz waves are in high demand because of their compact size and high sensitivity. THz devices have a wide range of applications, including broadcasting, satellite/mobile communications, explosive/weapon identification (including explosive/weapons identification systems), multimedia, environmental sensing (including radars), and medical systems [5]. Due to the wide range of possible applications, there has been a massive amount of study and technological improvement during the previous few decades. Consequently, the need for improved antennas that operate at terahertz (THz) frequencies is becoming more important [4]. It may be accomplished by developing tiny high-performance antennas that can send and receive signals in the terahertz frequency ranges, which will aid in the general development of future sophisticated terahertz communication systems. There is a substantial shortage of detectors and sources in the THz bands, which hinders the performance of devices operating in the terahertz domain. When using higher frequency bands (such as the THz band), you have access to more channel capacity, but you also have to increase the path loss and the sensitivity to blocking events. There is a consequent increase in the need for smaller antennas with high gain, high efficiency, and increased operational bandwidth to address these issues. With the need for ultrahigh-performance characteristic parameters for micro/nano-scaled THz antennas, many new difficulties and opportunities have arisen, all of which will undoubtedly contribute to the growth of antenna technology in the near term. There are many types of antenna design; for example, lens [6], photoconductive [7], horn [8], metamaterial [9], leaky-wave [10], on-chip [11], dielectric [12], and metallic antennas [13] are reported in the literature. Larger size and a complicated design procedure are required for these antennas to function. It is also challenging to incorporate these THz antenna designs with planar electronics. For their part, microstrip antennas are becoming more prevalent as planar technology becomes more ubiquitous. Because of its various advantages, including low cost, design simplicity, light weight, and small size, terahertz short-range wireless applications are especially well suited to these devices. However, despite its numerous advantages, it has limited bandwidth, preventing it from being used at high THz frequencies. To overcome this obstacle, tiny, lightweight antennas with a large operational bandwidth are being developed to enable various applications in the THz frequency region. Researchers have constructed and published various miniature THz antennas in the literature. However, they can only operate with extremely narrow bandwidths because of their small size [14–16]. In addition, in ref. [17], an investigation and proposal for a multi-layer array antenna are made. The THz antenna topologies presented herein enhance operational bandwidth in order to compensate for the larger antenna diameter. Wideband THz antennas were designed by researchers who published their results in peer-reviewed publications, with the intention of addressing the fading issue in high-speed, short-range wireless applications running at high frequencies in the THz spectrum. Use of multiple-input multiple-output (MIMO) antenna methods may minimize signal fading concerns in wireless networks.

In this work, an ultra-wideband graphene-based circular patch-shaped Yagi-like MIMO antenna is numerically investigated for 1–30 THz of the band. The various parameters, such as return loss, directivity, peak gain, TARC, ECC, MEG, CCL, and DG are calculated for the 2 $\times$ 2 MIMO antenna structure. The effect of the different antenna configurations—such as 1 $\times$ 2, 2 $\times$ 1 and 1 $\times$ 1 structures—has also been calculated to identify the influential operating bands. This design provides promising results for all the antenna parameters, making it suitable for THz wireless communication applications. The highlights of the proposed UWB antenna are as follows:

- Microstrip technology is used to design the graphene-based circular patch-shaped Yagi-like ultra-wideband MIMO antenna. Thus, it is smaller, lighter, easier to build, and more cost effective than other THz antennas.
- The suggested antenna has a substantially broader bandwidth (10.96 THz).
- The proposed MIMO structure offers better diverse performance parameters: DG $\approx$ 10 dB, CCL < 0.5 bps/Hz/s, TARC ≤ -10.0 dB, MEG ≤ -3.0 dB, and ECC < 0.01). This helps to overcome the challenges associated with short-distance communication such as signal fading, multipath propagation, and increased interference.

2. Graphene-Based Circular Patch-Shaped Yagi-like MIMO Antenna

The MIMO antenna with Yagi-like structure using graphene patch geometries is shown in Figure 1. Figure 1a shows the 4-port 2 $\times$ 2 MIMO antenna 3D view, with circular-patched geometry arranged in a Yagi-like structure. The antenna geometry has been formed using graphene material with a thickness of 0.03 μm. The conductivity of the graphene sheet was set as 10^8 S/m, with a loss tangent of 0.004. Because of its exceptional electromagnetic, mechanical, and tunable qualities, graphene material is widely employed in a wide range of Terahertz (THz) applications [18,19]. However, various articles have also observed that the multilayered graphene ink/powder does not provide great tunability. Hence, the fixed conductivity constant is considered for the overall structure. The overall size of the antenna is set as L × W = 620 × 800 μm^2. The design equation for the proposed antenna structure is given in Appendix B. The polyamide substrate thickness is 16 μm, with a loss tangent of 0.004 and a dielectric constant of 4.3 [20,21]. The dimensions of the structure are shown in Table 1. The dimensions shown in the structure were calculated by considering the wavelength of 1 THz signal (~300 μm for a single radiating element). The other dimensions were calculated by placing the periodic Yagi-like structure at an equal distance. The radius of the circular patch is set from small to large to couple all the small and large frequencies.

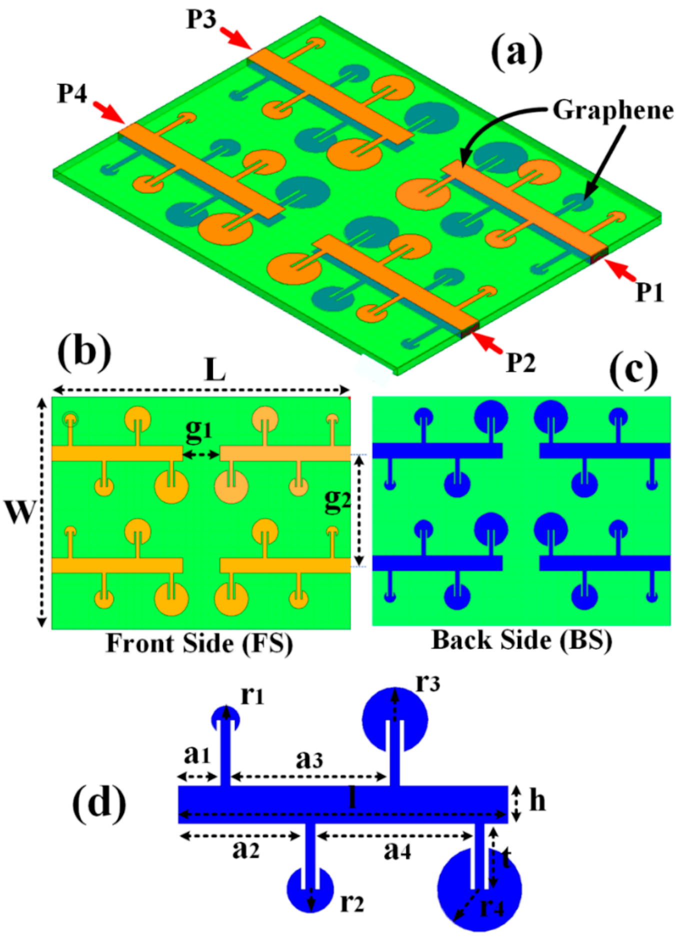

Figure 1. Schematic of the circular-patched Yagi-like THz MIMO antenna structures. (**a**) Three-dimensional view of the antenna, with graphene as the conducting material with Port notation. (**b**) Front side and backside view of the antenna. (**c**) A comprehensive view of the patched Yagi-like structure, with dimensions. (**d**) Schematic of the single antenna with dimensions.

Table 1. Dimensions of the 2 × 2 MIMO antenna structure (all dimensions in μm).

a1	a2	a3	a4	r1	r2	r3	r4	h	l	t	g1	g2
50	140	180	180	15	25	35	45	40	350	70	100	350

3. Results and Discussion

In this research, the various antenna structures were simulated to identify the optimized results for the MIMO antenna. We have investigated the five types of antenna structures. The proposed antenna and its various sub-designs (Types), as shown in Table A1, were numerically investigated using the HFSS Electromagnetic simulator tool. These antennas were simulated by considering 7.5 THz of the resonating frequency. Figures 2 and 3 show the variation in S parameters for the different port excitation of Type 1 (2 × 2) MIMO design. Figure 2a,b shows the variation in the S parameters while exciting port 1 and port 2 for 1–30 THz of the frequency band. Similarly, Figure 3a,b shows the variation in S parameters for port 3 and port 4 excitation. The detailed comparative results are shown in Table 2 for different port excitations. In all the port excitation conditions, three operating bands were observed, with a wide band of accepted return loss. In port 1 excitation, the maximum bandwidth ($S_{11} < -10$ dB) was observed at 10.02 THz, with maximum return loss on band 3 with −23.44 dB, while the minimum bandwidth observed in port 1 excitation was 0.63 THz. In port 2 excitation, the maximum operating bandwidth ($S_{22} < -10$ dB) was observed at 9.12 THz, with −22.55 dB of the minimum return loss. Similarly, in port 3 and port 4 excitation, the maximum bandwidth was observed at ($S_{33} < -10$ dB) 10.86 THz and ($S_{44} < -10$ dB) 10.96 THz, with −26.59 dB and −18.85 dB of the return loss, respectively. The directivity with co-polarization and cross-polarization is shown in Figure 4a.

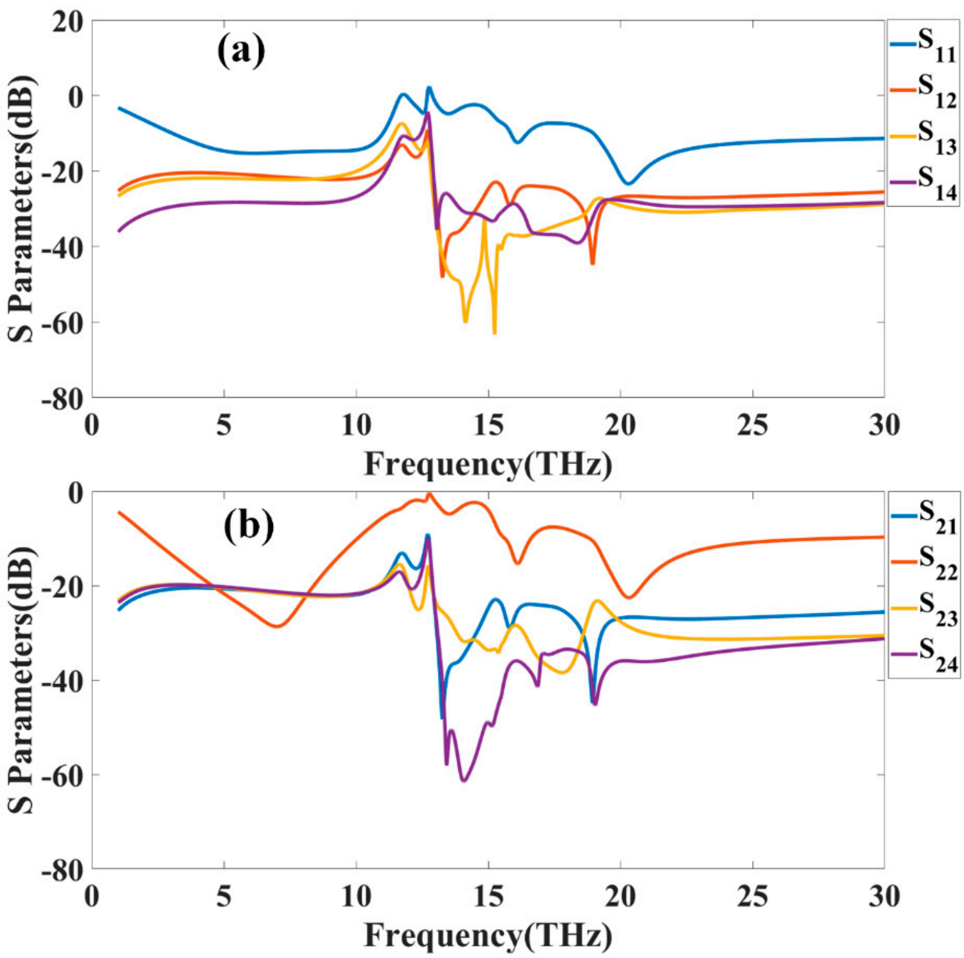

Figure 2. Calculated S-parameters for the Type-1 antenna (2 × 2 structure) by considering (**a**) port-1 and (**b**) port-2 as exciting ports.

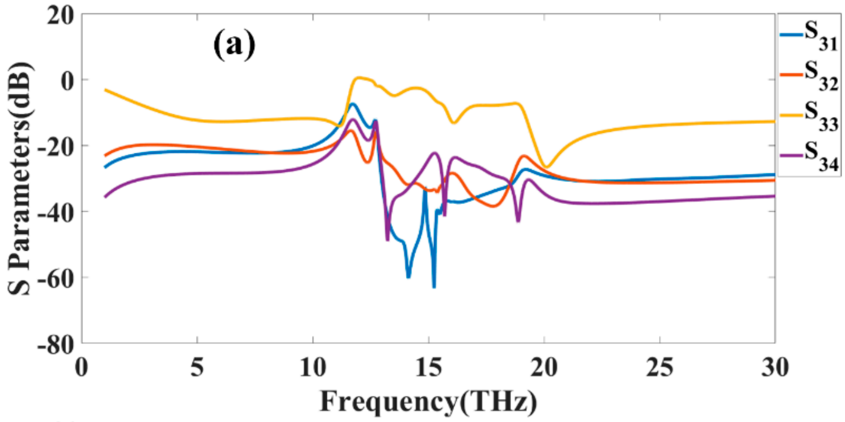

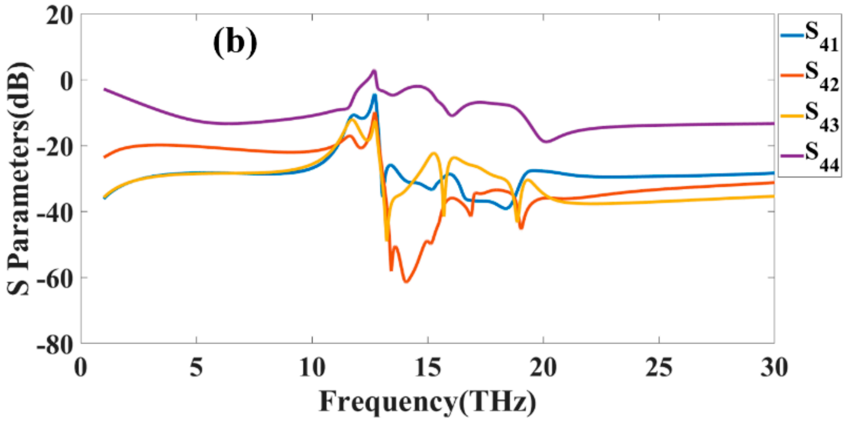

Figure 3. Calculated S-parameters for the Type-1 antenna (2 × 2 structure) by considering (**a**) port-3 and (**b**) port-4 as exciting ports.

Table 2. Comparative analysis of type 1 antenna for individual port excitation.

Port Excitation	Number of Bands	Minimum and Maximum Frequency (THz)	Bandwidth (THz)	Maximum Return Loss (dB)
Port 1	1	3.05–11.01	7.96	−15.31
	2	15.85–16.47	0.63	−12.49
	3	19.98–30	10.02	−23.44
Port 2	1	2.26–10.04	7.78	−28.67
	2	15.63–16.61	0.98	−15.38
	3	18.84–27.96	9.12	−22.55
Port 3	1	3.51–11.43	7.92	−14.13
	2	15.82–16.51	0.69	−13.19
	3	19.14–30	10.86	−26.59
Port 4	1	3.68–10.52	6.84	−13.29
	2	15.88–16.24	0.36	−11.93
	3	19.04–30	10.96	−18.85

Similarly, the three-dimensional directivity is shown in Figure 4b. To derive the results, only port 4 of the Type 1 antenna is excited while the other port excitation is considered zero. It can be observed from Figure 4 that co- and cross-polarization both provide the bidirectional high gain response in single-port excitation conditions. Figure 4b shows that the maximum gain is 6.32 dB in this single-port excitation condition. We have also calculated the effect in return loss, gain, and directivity for the other antennas, as shown in Table A1. These antennas' return loss and directivity are shown in Figures A1–A3. These results have helped us to choose the correct configuration of 2 × 2. While calculating the results of the 1 × 2, we found the results of an oscillator instead of an antenna, where return loss S11 > 0 in some of the cases. This band is generally observed between 15 and

20 THz in type 2 antennas. These results are not considered as standard antenna operation. Hence, the placement of the MIMO antenna in 1×2 mode is not suitable for wideband operation. In another type of result with 2×1, return loss results were observed as per the standard antenna calculations S11 < 0. The same acceptable results are also observed in 1×1 geometry. This analysis will generate the 2×2 antenna structure, where these oscillating effects are reduced and the antenna operates in a wide band. As shown in Figures 2 and 3, some bands generally show minor oscillating effects between 10 and 17.5 THz. In comparison, for the rest of the band, the proposed antenna structure provides an acceptable return loss, with significantly fewer values of cross-port S parameter (S12, S13, S14, S21...) responses. The effect of the radius of the circular patch in return loss is shown in Figure 5. These results are derived for r1 = r2 = r3 = r4 = 2 µm. The S11 < −10 dB values are observed in the majority of cases. The cross-polarization gain is reduced, but co-polarization gain is >3 dB at 7.5 THz of the frequency. This can help us to identify the optimized results for the overall structure. The variation in radius of the patch makes the co- and cross-polarization gain better than the same radius patch structure. The calculated gain for the different antenna types is shown in Figure 6. Figures 7–9 show the variation in gain for the different port excitement conditions and polarization angles. In the simulation environment, the port is excited with different conditions: one-port, two-port, three-port, and all-port excitation. In the case of one-port excitation, the other port is considered no feeding, with the condition of lumped port excitation zero. As shown in Figure 6, the other antenna elements have lower surface current density distribution. This surface current density and impedance matching condition generated the overall gain pattern from the antenna, which was different from two- and higher-number port excitations. We observed that the gain pattern lobes depend on the number of the exciting ports. These results can help identify the variation in directivity with maximum gain for the different port excitation conditions. The various gain-forming conditions using different port excitations are varied in surface conductivity and directivity changes in 2D and 3D. In a real-time application, individual ports excited by the matching circuits and the non-excited port can be connected to matched terminator devices. As shown in Table 2, an average of 7.5 dB gain was observed in the majority of the bands for the type 1 antenna. Due to the oscillating effects, the gain is higher in the 11–15 THz range, but return loss is not the standard antenna parameter. Thus, this band can neglect overall antenna operations. The different antenna MIMO analysis parameters such as MEG, CCL, ECC, DG, and TARC have been calculated for the proposed type 1 antenna. The ECC parameter correlates far-field radiation patterns induced at different ports of the MIMO architecture. An ECC of 0.5 or below is required for any MIMO architecture [22,23]. ECC can be calculated using electric field magnitude, as shown in Equation (1). The ECC of the antenna and jth components of the system is represented by ρ_{ij}, whilst the solid angle is represented by Ω. The assessment of ECC based on far-field radiation factors is a time-consuming and complicated process. Another technique for determining ECC using the S parameter approach is described in Equation (2), as published in [24].

$$\rho_{ij} = \left| \frac{\iint \left(E_{\theta_i} \cdot E^*_{\theta_j} + E_{\varphi} : E^*_{\varphi_j} \right)^{d\Omega}}{\iint \left(E_{\theta_i} \cdot E^*_{\theta_i} + E_{\varphi_i} \cdot E^*_{\varphi_i} \right) d\Omega \iint \left(E_{\theta_j} \cdot E^*_{\theta_j} + E_{\varphi_j} \cdot E^*_{\varphi_i} \right)^{d\Omega}} \right|^2 \tag{1}$$

$$\rho_{ij} = \frac{\left| S^*_{11} S_{12} + S^*_{21} S_{22} \right|^2}{\left(1 - \left(|S_{11}|^2 + |S_{21}|^2 \right) \right) \left(1 - \left(|S_{22}|^2 + |S_{12}|^2 \right) \right)} \tag{2}$$

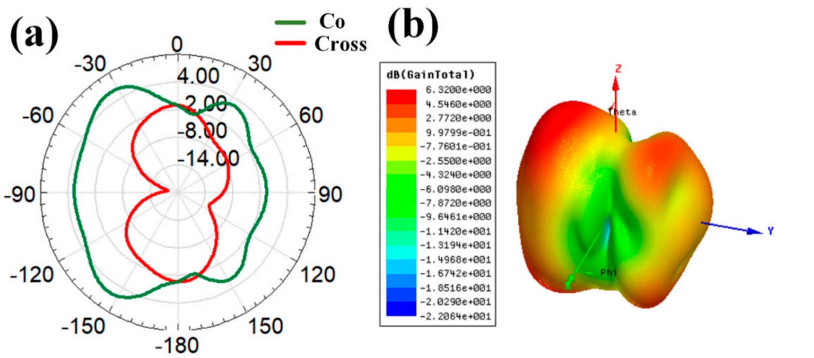

Figure 4. Directivity response for the Type-1 antenna under the consideration of port-1 as an exciting port. (**a**) 2D response of directivity with co- and cross-polarization. (**b**) 3D directivity response.

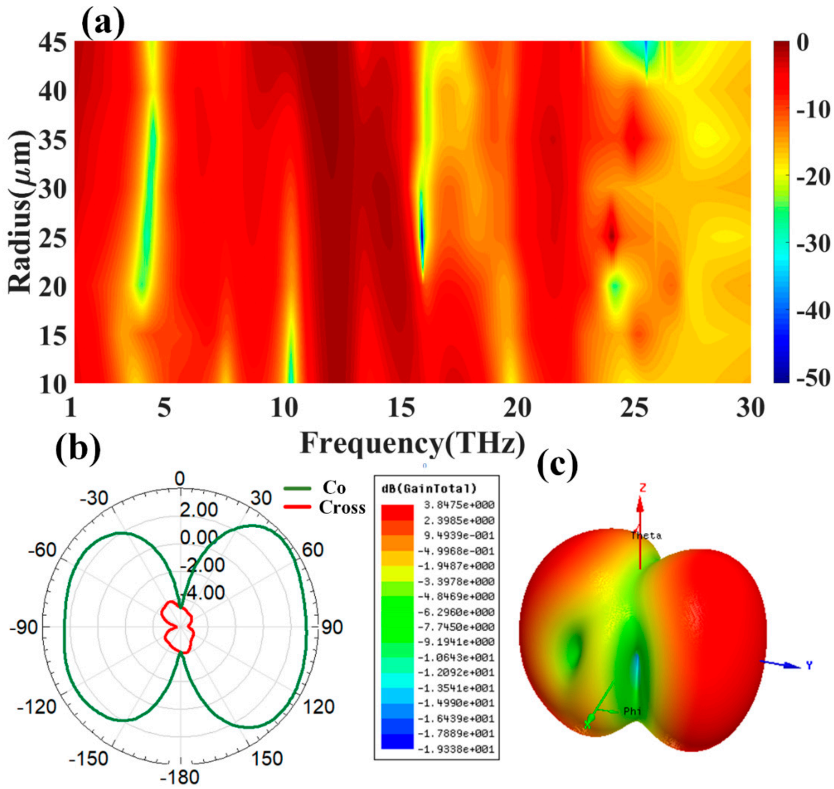

Figure 5. (**a**) Variation in S-parameters (S11) for the different radius values for type-5 antenna. Calculated directivity in (**b**) 2D (with co- and cross-polarization) and (**c**) 3D, by considering a radius of 20 μm.

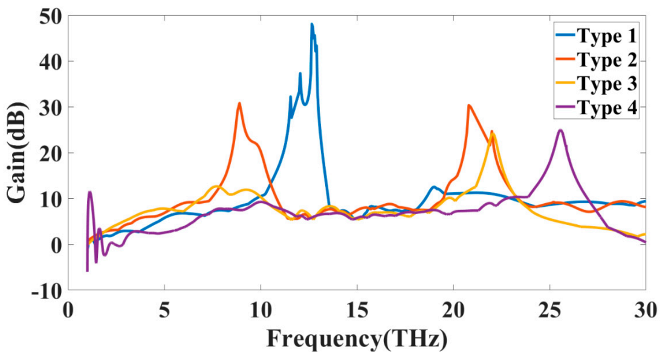

Figure 6. Calculated gain for the different types of antenna.

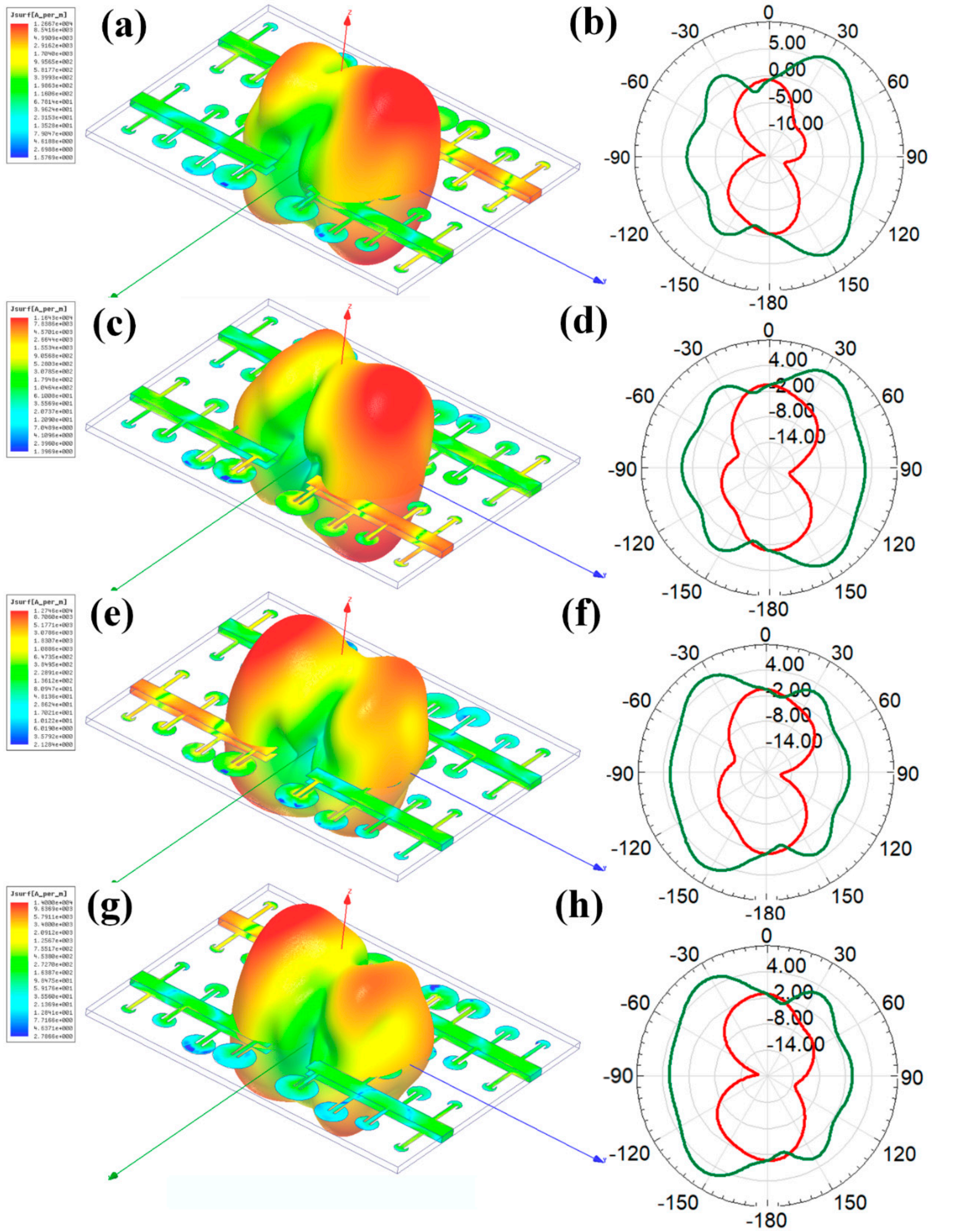

Figure 7. Variation in gain for the different modes of port excitation, along with co- and cross-polarization effects. Three-dimensional directivity with co- and cross-polarization for port excitation conditions of (P1, P2, P3, P4): (**a**) (1, 0, 0, 0), (**c**) (0, 1, 0, 0), (**e**) (0, 0, 1, 0), and (**g**) (0, 0, 0, 1). Two-dimensional directivity with co- and cross-polarization for port excitation conditions of (P1, P2, P3, P4): (**b**) (1, 0, 0, 0), (**d**) (0, 1, 0, 0), (**f**) (0, 0, 1, 0), and (**h**) (0, 0, 0, 1). co- (green line) and cross-polarization (red line).

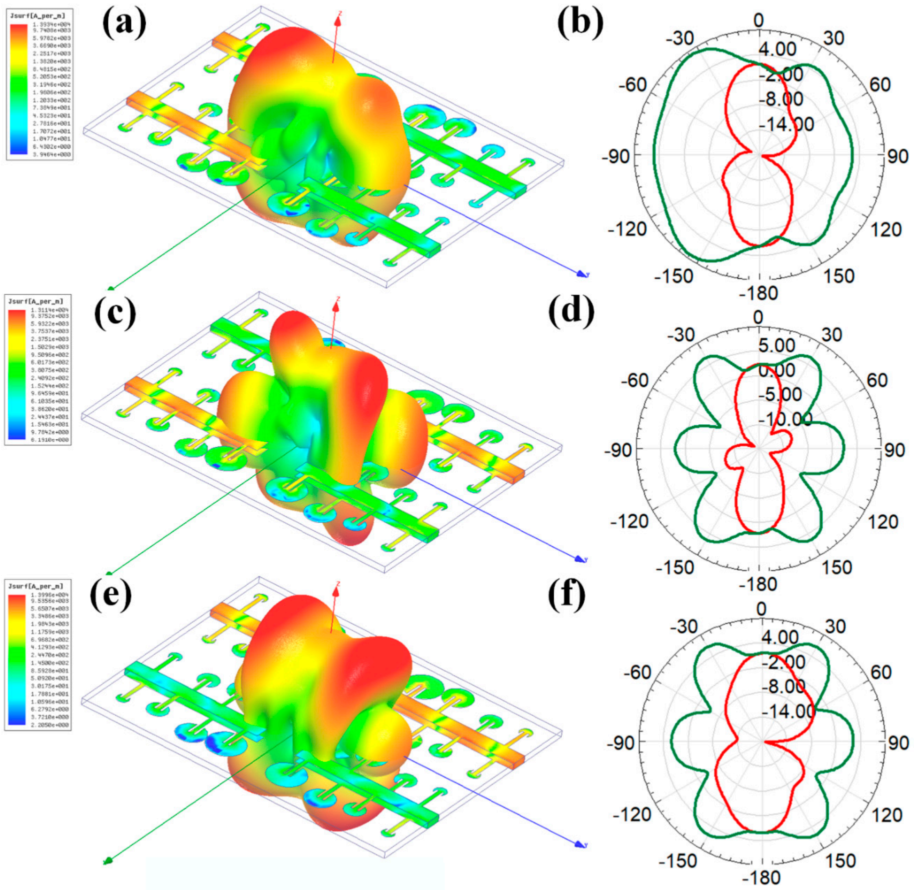

Figure 8. Variation in gain for the different modes of port excitation, along with co- and cross-polarization effects. Three-dimensional directivity with co- and cross-polarization for port excitation conditions of (P1, P2, P3, P4): (**a**) (0, 0, 1, 1), (**c**) (1, 0, 0, 1), and (**e**) (1, 0, 1, 0). Two-dimensional directivity with co- and cross-polarization for port excitation conditions of (P1, P2, P3, P4): (**b**) (0, 0, 1, 1), (**d**) (1, 0, 0, 1), and (**f**) (1, 0, 1, 0). co- (green line) and cross-polarization (red line).

Figure 10a depicts the relationship between ECC and frequency for the suggested type 1 antenna for the different port excitations. On the other hand, it can be noticed that the ECC of the antenna remains below 0.001 over its whole operational bandwidth (1–10 THz and 15–30 THz). These ECC values make the system stable. The lower value of the ECC obtained suggests less correlation between the antenna components themselves. The values are much lower than the allowed limit of 0.5, ensuring that the suggested antenna would provide satisfactory MIMO performance. Fading is reduced by combining antenna components that have distinct fading characteristics. To calculate diversity gain [23], one must compare a diversity antenna system to its equivalent single diversity antenna system in a given channel and determine the difference in signal-to-noise ratio. DG may be evaluated in terms of a theoretical maximum diversity gain of 10 dB and an envelope correlation coefficient, as shown in Equation (8). The MIMO antenna patch components are more isolated when the diversity gain increases. In other words, the DG should be at least 9 dB higher than that. The estimated DG values are over 20 dB over all three working bands of the antenna, as shown in Figure 10d. This assures that the suggested MIMO structure diversity performance is good.

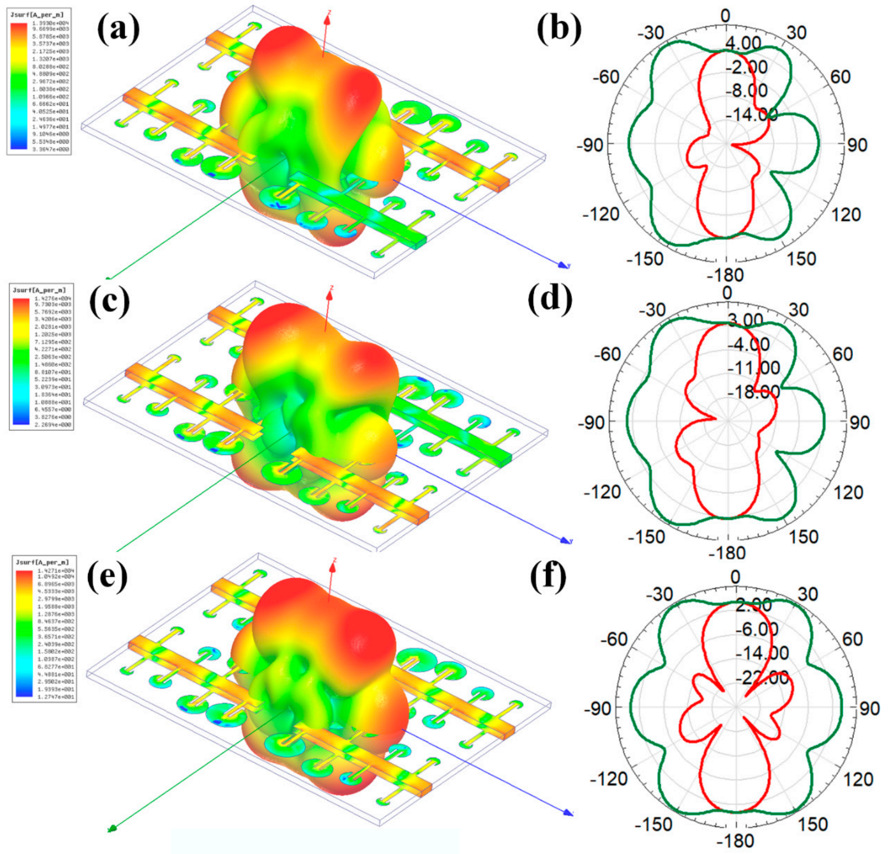

Figure 9. Variation in gain for the different modes of port excitation, along with co- and cross-polarization effects. Three-dimensional directivity with co- and cross-polarization for port excitation conditions of (P1, P2, P3, P4): (**a**) (1, 0, 1, 1), (**c**) (0, 1, 1, 1), and (**e**) (1, 1, 1, 1). Two-dimensional directivity with co- and cross-polarization for port excitation conditions of (P1, P2, P3, P4): (**b**) (1, 0, 1, 1), (**d**) (0, 1, 1, 1), and (**f**) (1, 1, 1, 1). co- (green line) and cross-polarization (red line).

Antenna diversity methods, which combine antenna parts that suffer from various types of fading, are used to lessen the effect of fading. By applying the DG equation [23], as shown in Equation (8), the maximum theoretical diversity gain (10 dB) and the envelope correlation coefficient may be evaluated for this value (8). In MIMO antennas, a more considerable diversity gain indicates more isolation between the patch components, which is indicated by a lower value of diversity gain. To be considered loud, the DG must be more than 20 dB. In Figure 10d, it can be seen that the estimated values of DG over 20 dB over the whole working range of the antenna. As a result, the suggested MIMO structure has excellent diversity performance. The MEG parameter indicates that the amount of average power received by a diversity antenna in the presence of noise is greater than the sum of average powers received by two isotropic antennas in the absence of noise (or interference). It depicts the performance increase of a MIMO antenna while considering the impacts of the surrounding environment. We can determine whether the MEG is present at both ports of the planned structure by utilizing Equation (4), as shown in [25].

$$DG = 10\sqrt{1-|ECC|^2} \tag{3}$$

$$\mathrm{MEG}_i = 0.5\eta_{i,\mathrm{rad}} = 0.5[1 - \sum_{j=1}^{M} |Sij|^2] \tag{4}$$

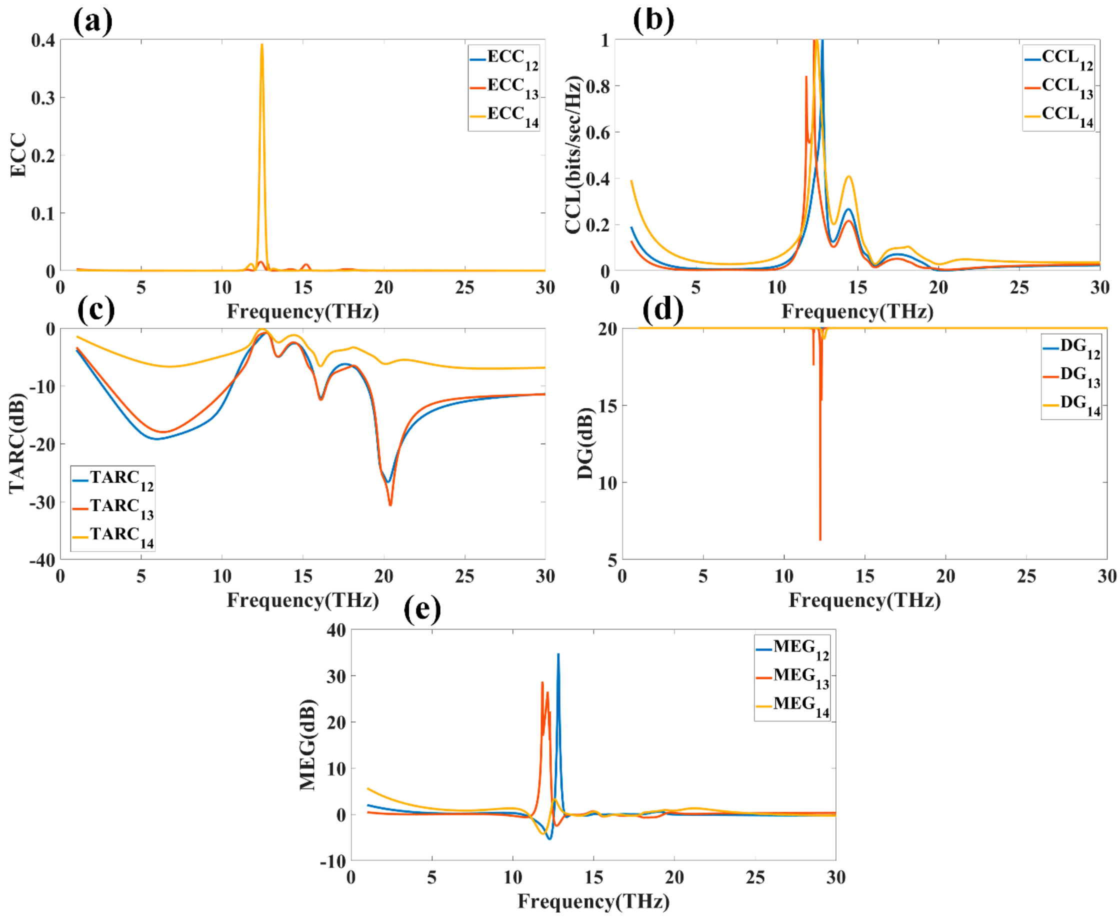

Figure 10. Different calculated parameters for the 2 × 2 MIMO antenna structure: (**a**) ECC, (**b**) CCL, (**c**) TARC, (**d**) DG, and (**e**) MEG.

In Equation (4), M denotes the total number of ports in the MIMO design, while $\eta_{i,\text{ rad}}$ denotes the radiation efficiency of the existing MIMO design structure. The value of MEG should be −3 dB to achieve better diversity performance at each port of the device. Making the difference between the two ports around 0 dB is also required. Figure 10e shows the values of MEG < −3 dB for all three operating modes. TARC is the optimum measure to describe radiation performance and frequency response when used in more than one port. It is the square root of total reflected power divided by total incident power in a MIMO system. TARC measures how effective a MIMO system refracts light. When calculating TARC, mutual coupling and random signal pairings between ports on the network are considered. Equation (5) shows how reflected and incident waves describe it. Equation (6) in terms of S parameters, as stated in [26], may also be used to calculate this. Figure 10c shows the variation in the TARC of the proposed MIMO antenna. Acquired data has been deemed suitable for intended applications in terms of THz band MIMO performance.

$$\Gamma_a^t = \frac{\sqrt{\sum_j^M |b_j|^2}}{\sum_j^M |a_j|^2} \tag{5}$$

$$\Gamma_a^t = \sqrt{\frac{\left|S_{11} + S_{12}e^{j\theta}\right|^2 + \left|S_{21} + S_{22}e^{j\theta}\right|^2}{2}} \tag{6}$$

$$C_{loss} = -log_2\, det\left(a^R\right) \tag{7}$$

$$a^R = \begin{pmatrix} \rho_{11} & \rho_{12} \\ \rho_{21} & \rho_{22} \end{pmatrix} \tag{8}$$

$$\rho_{ii} = 1 - \left(|S_{ii}|^2 + |S_{ij}|^2\right),\ and\ \rho_{ij} = -\left(s_{ii}^* S_{ij} + s_{ij}^* S_{ij}\right),\ where\ i, j = 1 \text{ or } 2 \tag{9}$$

Another essential characteristic to consider while evaluating the MIMO performance of the planned THz antenna is the CCL. The channel capacity loss defines the maximum rate at which information may be sent without substantial loss. The rate should be less than 0.5 bits/s/Hz to demonstrate lossless information transfer in a well-designed MIMO system. It is possible to calculate the CCL parameter using Equations (7)–(9) presented in [26]. This CCL limit is also satisfied as per the results shown in Figure 10b. Table 2 shows the comparative analysis between the proposed structure and previously published structure in terms of dimension, gain, and material used for designing the antenna. It can be observed from the comparative analysis structure that the proposed antenna provides the ultra-wideband of 10.96 THz, with an approximate average gain of 7 dB. This design also provides better values of the MIMO parameters CCL, DG, Gain, TARC, ECC, and MEG.

Comparative analysis of proposed antenna in terms of gain, dimension, bandwidth and substrate material with previously published results is shown in Table 3.

Table 3. Comparative analysis of the proposed structure with previously published articles.

Reference	Substrate	Gain (dB)	Dimension (µm × µm)	Bandwidth (THz)
This work	Polyimide	~7	(620, 800)	10.96
[27]	Tetrafluoroethylene	-	(109.76, 150.93)	0.13
[28]	RT/Duroid 6006	9.7	(600, 700)	0.15
[29]	Pyrex	7.3	(500, 500)	-
[30]	RT/Duroid 6006	3.09	(1000, 1000)	0.15
[31]	Polyimide	9.19	(600, 600)	0.2
[32]	Polyimide	8	(600, 800)	0.0364
[28]	RT/Duroid 6006	9.7	(600, 700)	0.15
[33]	RT/Duroid 6006	10.43	(1000, 1000)	0.155
[28]	RT/Duroid 6006	9.7	(600, 700)	0.15
[34]	Photonic crystal	10.7	(500, 500)	-
[29]	Pyrex	7.3	(500, 500)	-
[27]	Tetraflouroethilen	-	(109.76, 150.93)	0.13
[35]	Polyimide	5.7	(300, 300)	0.269
[36]	Triethylamine	9.70	(400, 400)	0.119

Figure 11 shows the calculated impedance for the all-port antenna, with a frequency range impedance variation of 9–80 Ω at 1–10 THz. Similarly, an impedance variation of 25–110 Ω was observed at 15–20 THz. Therefore, we can apply the antenna's feeding using multiple methods that offer impedance variation through various parameters. For example, the sub-millimeter wave antenna feeding using a diagonal horn structure can be one of the methods to feed these types of antennas [37,38]. With its wide and thin walls running along the diagonals of the cross section of the pyramid, this feeder antenna has a horned section with a flared pyramid top. A second method for designing the mm-wave feeding uses a platelet conical corrugated structure [38,39]. Figure 12 shows the variation in S parameters by considering all-port excitation. The results show variations in individual port return loss and other active reflectance coefficient values. As shown in Figure 12, the return loss and other reflectance coefficient values are below −10 dB for all operating bands defined in Table 1. These results help us identify the active reflectance coefficient when all the ports are excited. The values of the active return loss of <−10 dB indicate the overall wave interference performance of the proposed antenna when it is entirely operated with all-port excitation.

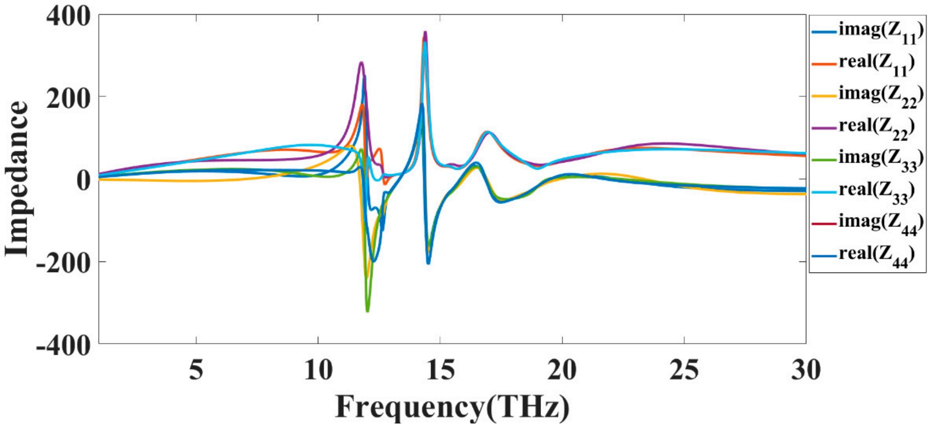

Figure 11. Calculated real and imaginary impedance values of the proposed MIMO antenna.

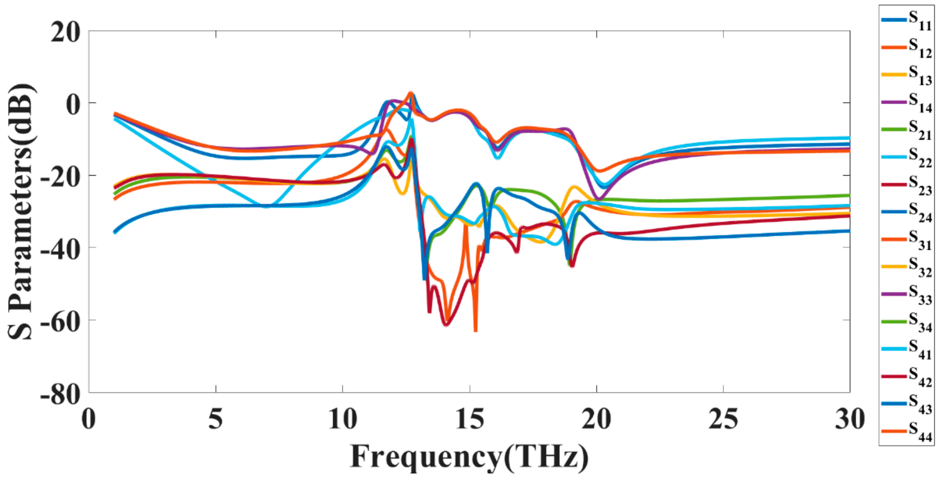

Figure 12. Calculated reflection coefficient of the proposed four-port structure. S parameters are calculated by exciting all four ports.

4. Conclusions

In this study, an ultra-wideband graphene-based circular patch-shaped Yagi-like MIMO antenna was numerically investigated for use in the applications of THz wireless communication. The reflectance coefficient, directivity, gain, and efficiency parameters have been analyzed for the proposed antenna. The feasibility of the MIMO antenna has also been investigated in terms of various parameters such as TARC, ECC, CCL, MEG, and DG. The proposed MIMO structure offers better diversity performance parameters. All these values under the 1–10 THz and 15–30 THz bands show acceptable standard values, which helps overcome the challenges associated with short-distance communication such as signal fading, multipath propagation, and increased interference. The suggested THz MIMO antenna provides the operating bands of 1–10 THz and 15–30 THz with good isolation values. This antenna offers an ultra-wideband of 10.96 THz of the bandwidth. All the MIMO antenna values are satisfied for the effective radiation operation in this range. Therefore, this MIMO antenna can work for high-speed short-distance indoor applications under the THz band.

Author Contributions: V.S. conceived the project, gathered all the supporting information, and supervised the overall project. A.G.A. computed the overall structure and generated the results. Both authors contributed equally to writing the manuscript. All authors have read and agreed to the published version of the manuscript.

Funding: This research received no external funding.

Data Availability Statement: All data are included within the manuscript.

Conflicts of Interest: The authors declare no conflict of interest.

Appendix A

The graphene-based circular patch-shaped Yagi-like MIMO antenna has been numerically investigated in the frequency range of 1–30 THz. The different antenna modes were initially investigated to identify the optimized results of the MIMO structure. Table A1 shows the different structures and types of the antenna simulated to check optimized results. Figures A1–A4 show the variation in the return loss, two-dimensional directivity, and three-dimensional directivity response.

Table A1. Types of MIMO antenna Configuration.

Types of Antenna	Types of Antenna	Configuration
Type 1	2 × 2	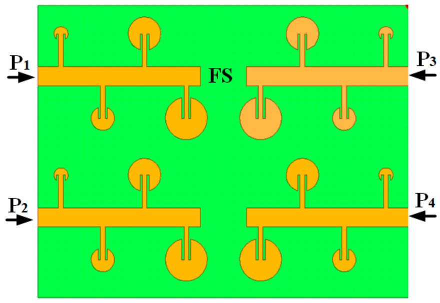
Type 2	1 × 2	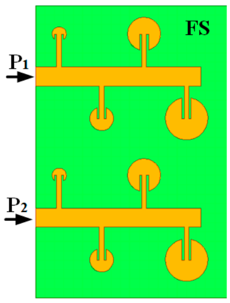
Type 3	2 × 1	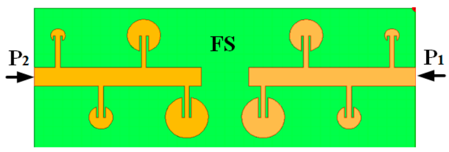
Type 4	1 × 1	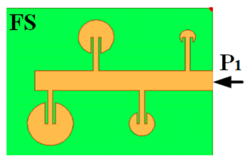
Type 5	All patch, one side	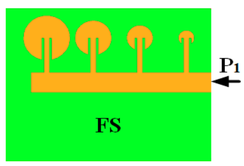

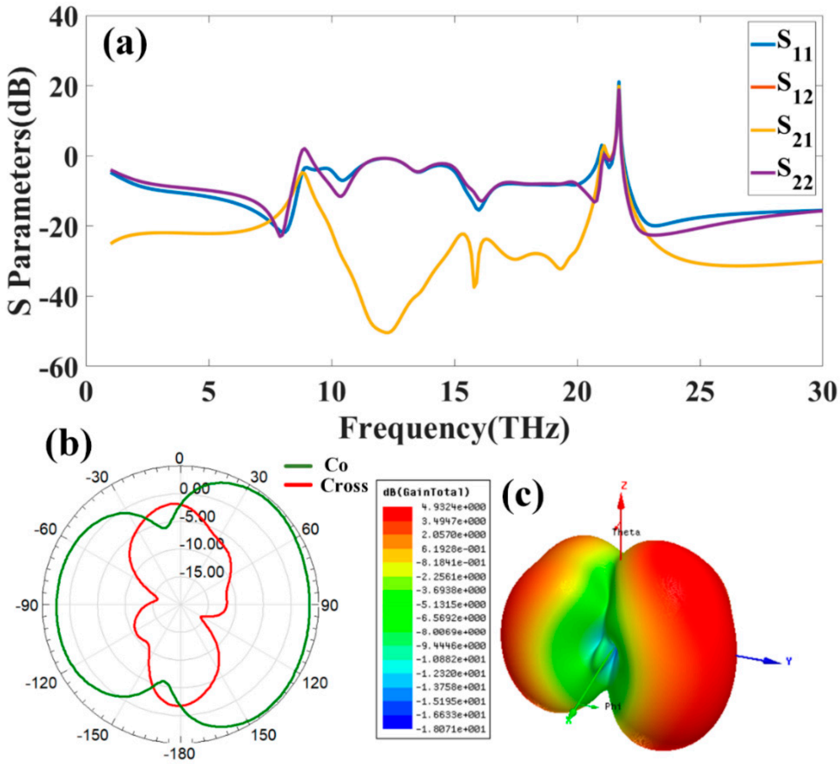

Figure A1. (**a**) Calculated S parameters for the type-2 antenna. Calculated directivity in (**b**) 2D (with co- and cross-polarization) and (**c**) 3D, by considering single-port (Port 1) excitation.

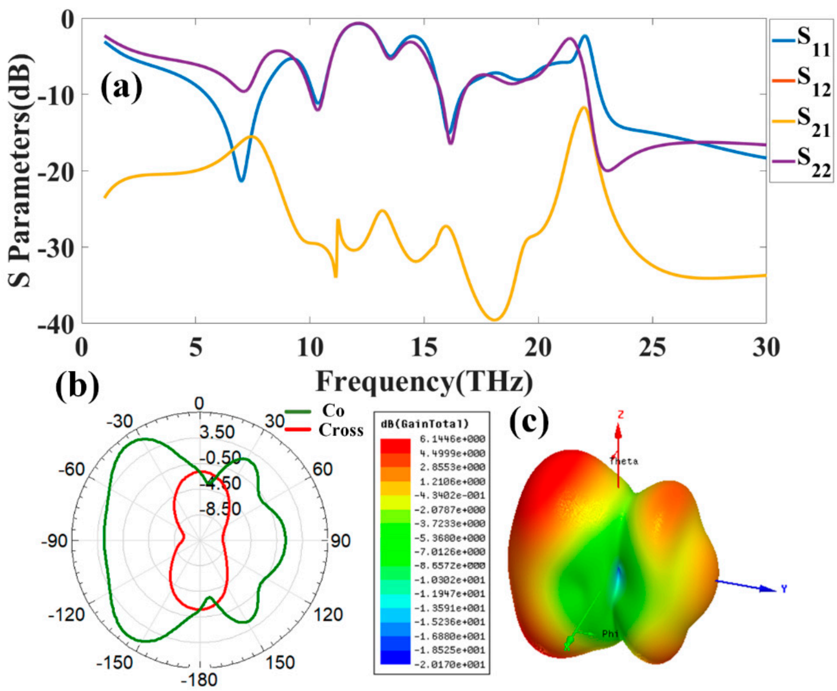

Figure A2. (**a**) Calculated S-parameters for the type-3 antenna. Calculated directivity in (**b**) 2D (with co- and cross-polarization) and (**c**) 3D, by considering single-port (Port-1) excitation.

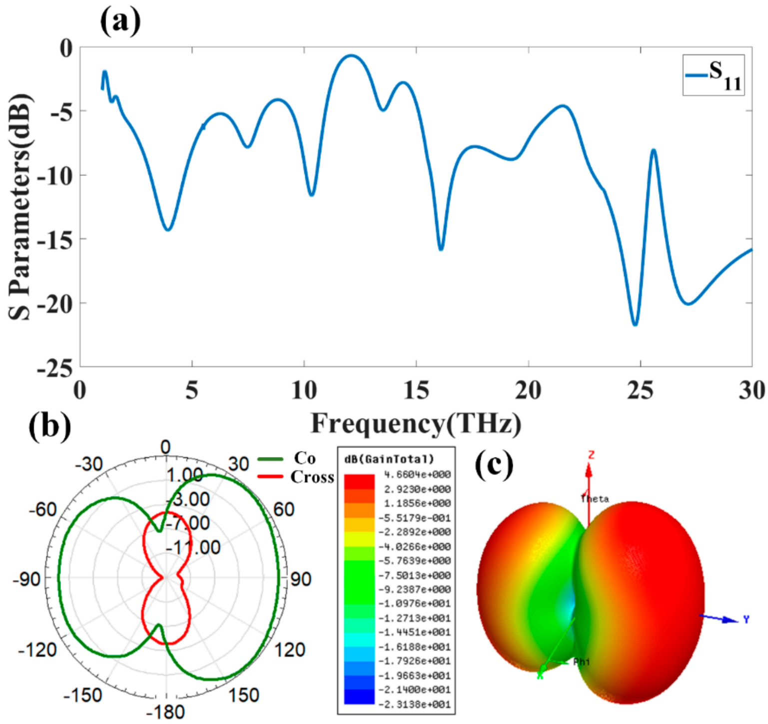

Figure A3. (**a**) Calculated S-parameters for the type-4 antenna. Calculated directivity in (**b**) 2D (with co- and cross-polarization) and (**c**) 3D, by considering single-port (Port-1) excitation.

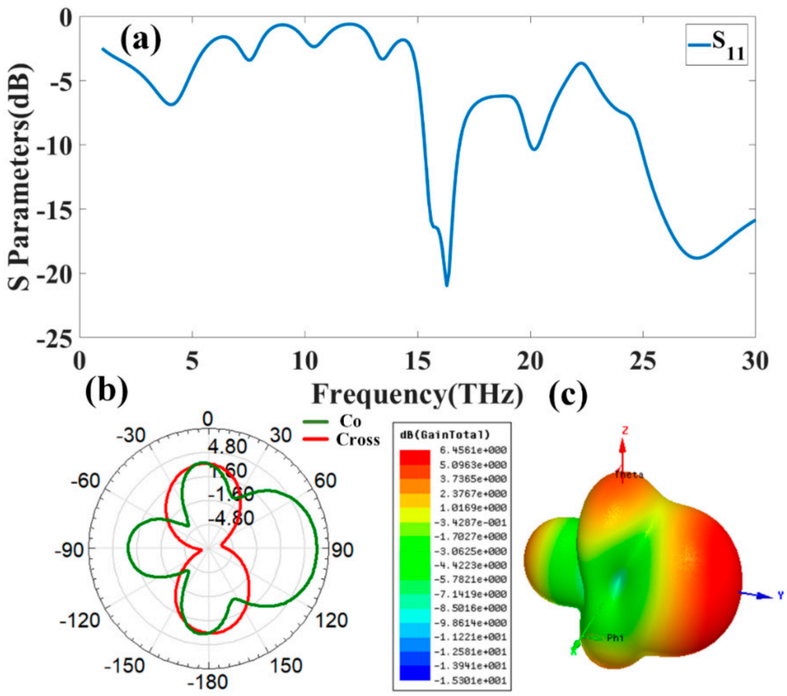

Figure A4. (**a**) Variations in S-parameters (S11) for the structure were all circular patched structures in a one-sided (Type-5) antenna. Calculated directivity in (**b**) 2D (with co- and cross-polarization) and (**c**) 3D, with a maximum directivity of 6.45 dB.

Appendix B

The proposed MIMO antenna is designed using the formula for calculating the minimum and maximum size of the dipole elements in the antenna [40]. The maximum (L_{max}) and minimum L_{min} length of the dipole element can be calculated using $L_{max} = \frac{c}{f_{min}\sqrt{\varepsilon_r}}$ and

$L_{min} = \frac{c}{f_{max}\sqrt{\varepsilon_r}}$. Here, C is the velocity of light, ε_r is the permittivity of the substrate, f_{min} is the minimum frequency, and f_{max} is the maximum frequency. We have calculated the minimum and maximum length of the dipole element to be 7.2 µm and 144 µm, respectively. According to this calculation, we have set the dipole's overall length as 2 × t = 140 µm. In this design case, the substrate is not the only material where EM waves become confined. Therefore, the practical permittivity calculation is required to be calculated again for the overall dimensions of the structure. We have to use the microstrip line formula $\varepsilon_{eff} = \frac{\varepsilon_r+1}{2} + \frac{\varepsilon_r-1}{2}\left[1+12\frac{h}{l}\right]^{-1/2}$ to identify the size of the structure. Here, h and l are the thickness of the substrate and the length of the feed line, respectively. The calculated ε_{eff} is ~12.22. The overall structure size is calculated by $L = \frac{\lambda_{max}}{4}\left(1-\frac{1}{B_s}\right)\cot\alpha$. Here, B_s is the desired bandwidth, and α is 12.132° to achieve an approximate gain of 8 dB. Overall, the value of the length obtained is 310 µm. These design criteria are considered for single-antenna radiation. The overall dimensions increase to 620 × 800 µm^2, including the spacing between two MIMO elements and a circular patch.

References

1. Cisco: Cisco Visual Networking Index (VNI) Global Mobile Data Traffic Forecast Update, 2017–2022 White Paper. 2019. Available online: https://www.gsma.com/spectrum/wp-content/uploads/2013/03/Cisco_VNI-global-mobile-data-traffic-forecast-update.pdf (accessed on 10 March 2022).
2. Ying, Z. Antennas in Cellular Phones for Mobile Communications. *Proc. IEEE* **2012**, *100*, 2286–2296. [CrossRef]
3. Rappaport, T.S.; Sun, S.; Mayzus, R.; Zhao, H.; Azar, Y.; Wang, K.; Wong, G.; Schulz, J.K.; Samimi, M.; Gutierrez, F. Millimeter Wave Mobile Communications for 5G Cellular: It Will Work! *IEEE Access* **2013**, *1*, 335–349. [CrossRef]
4. He, Y.; Chen, Y.; Zhang, L.; Wong, S.-W.; Chen, Z.N. An overview of terahertz antennas. *China Commun.* **2020**, *17*, 124–165. [CrossRef]
5. Singh, R.; Lehr, W.; Sicker, D.; Huq, K.M.S. Beyond 5G: The Role of THz Spectrum. *SSRN Electron. J.* **2019**. [CrossRef]
6. Formanek, F.; Brun, M.-A.; Umetsu, T.; Omori, S.; Yasuda, A. Aspheric silicon lenses for terahertz photoconductive antennas. *Appl. Phys. Lett.* **2009**, *94*, 021113. [CrossRef]
7. Saurabh, L.; Bhatnagar, A.; Kumar, S. Design and performance analysis of bow-tie photoconductive antenna for THz application. In Proceedings of the 2017 International Conference on Intelligent Computing and Control (I2C2), Coimbatore, India, 23–24 June 2017; Volume 2018, pp. 1–3.
8. Gonzalez, A.; Kaneko, K.; Kojima, T.; Asayama, S.; Uzawa, Y. Terahertz Corrugated Horns (1.25–1.57 THz): Design, Gaussian Modeling, and Measurements. *IEEE Trans. Terahertz Sci. Technol.* **2017**, *7*, 42–52.
9. Devapriya, A.T.; Robinson, S. Investigation on Metamaterial Antenna for Terahertz Applications. *J. Microwaves Optoelectron. Electromagn. Appl.* **2019**, *18*, 377–389. [CrossRef]
10. Mak, K.-M.; So, K.-K.; Lai, H.-W.; Luk, K.-M. A Magnetoelectric Dipole Leaky-Wave Antenna for Millimeter-Wave Application. *IEEE Trans. Antennas Propag.* **2017**, *65*, 6395–6402. [CrossRef]
11. Khamaisi, B.; Jameson, S.; Socher, E. A 210–227 GHz Transmitter With Integrated On-Chip Antenna in 90 nm CMOS Technology. *IEEE Trans. Terahertz Sci. Technol.* **2013**, *3*, 141–150. [CrossRef]
12. Varshney, G. Tunable Terahertz Dielectric Resonator Antenna. *Silicon* **2021**, *13*, 1907–1915. [CrossRef]
13. Zhou, M.M.; Cheng, Y.J. D-Band High-Gain Circular-Polarized Plate Array Antenna. *IEEE Trans. Antennas Propag.* **2018**, *66*, 1280–1287. [CrossRef]
14. Dhillon, A.S.; Mittal, D.; Sidhu, E. THz rectangular microstrip patch antenna employing polyimide substrate for video rate imaging and homeland defence applications. *Optik* **2017**, *144*, 634–641. [CrossRef]
15. Sirmaci, Y.D.; Akin, C.K.; Sabah, C. Fishnet based metamaterial loaded THz patch antenna. *Opt. Quantum Electron.* **2016**, *48*, 168. [CrossRef]
16. Paul, L.C.; Islam, M. Proposal of wide bandwidth and very miniaturized having dimension of µm range slotted patch THz microstrip antenna using PBG substrate and DGS. In Proceedings of the 20th International Conference of Computer and Information Technology (ICCIT), Dhaka, Bangladesh, 22–24 December 2017; Volume 2018, pp. 1–6. [CrossRef]
17. Vettikalladi, H.; Sethi, W.; Bin Abas, A.F.; Ko, W.; Alkanhal, M.A.; Himdi, M. Sub-THz Antenna for High-Speed Wireless Communication Systems. *Int. J. Antennas Propag.* **2019**, *2019*, 9573647. [CrossRef]
18. Geim, A. Graphene—The perfect atomic lattice. *Uspekhi Fiz. Nauk* **2011**, *181*, 1283.
19. Patel, S.K.; Sorathiya, V.; Nguyen, T.K.; Dhasarathan, V. Numerical investigation of tunable metasurface of graphene split-ring resonator for terahertz frequency with reflection controlling property. *Phys. E Low-Dimens. Syst. Nanostruct.* **2019**, *118*, 113910. [CrossRef]
20. Anand, S.; Kumar, D.S.; Wu, R.J.; Chavali, M. Graphene nanoribbon based terahertz antenna on polyimide substrate. *Optik* **2014**, *125*, 5546–5549. [CrossRef]

21. Thampy, A.S.; Darak, M.S.; Dhamodharan, S.K. Analysis of graphene based optically transparent patch antenna for terahertz communications. *Phys. E Low-Dimens. Syst. Nanostruct.* **2015**, *66*, 67–73. [CrossRef]
22. Babu, K.V.; Anuradha, B. Design of inverted L-shape & ohm symbol inserted MIMO antenna to reduce the mutual coupling. *AEU—Int. J. Electron. Commun.* **2019**, *105*, 42–53. [CrossRef]
23. Sree, G.N.J.; Nelaturi, S. Design and experimental verification of fractal based MIMO antenna for lower sub 6-GHz 5G applications. *AEU—Int. J. Electron. Commun.* **2021**, *137*, 153797. [CrossRef]
24. Babu, K.V.; Anuradha, B.; Das, S. Design & analysis of a dual-band MIMO antenna to reduce the mutual coupling. *J. Instrum.* **2019**, *14*, P09023. [CrossRef]
25. Nasir, J.; Jamaluddin, M.H.; Khalily, M.; Kamarudin, M.R.; Ullah, I.; Selvaraju, R. A reduced size dual port MIMO DRA with high isolation for 4G applications. *Int. J. RF Microw. Comput. Eng.* **2015**, *25*, 495–501. [CrossRef]
26. Sharawi, M.S. Printed Multi-Band MIMO Antenna Systems and Their Performance Metrics [Wireless Corner]. *IEEE Antennas Propag. Mag.* **2013**, *55*, 218–232. [CrossRef]
27. Azarbar, A.; Masouleh, M.S.; Behbahani, A.K. A new terahertz microstrip rectangular patch array antenna. *Int. J. Electromagn. Appl.* **2014**, *4*, 25–29.
28. Mahmud, R.H. Terahertz Microstrip Patch Antennas For The Surveillance Applications. *Kurd. J. Appl. Res.* **2020**, *5*, 16–27. [CrossRef]
29. Nejati, A.; Sadeghzadeh, R.A.; Geran, F. Effect of photonic crystal and frequency selective surface implementation on gain enhancement in the microstrip patch antenna at terahertz frequency. *Phys. B Condens. Matter* **2014**, *449*, 113–120. [CrossRef]
30. Sharma, A.; Singh, G. Rectangular Microstirp Patch Antenna Design at THz Frequency for Short Distance Wireless Communication Systems. *J. Infrared Millim. Terahertz Waves* **2008**, *30*, 1. [CrossRef]
31. Hocini, A.; Temmar, M.; Khedrouche, D.; Zamani, M. Novel approach for the design and analysis of a terahertz microstrip patch antenna based on photonic crystals. *Photonics Nanostruct.-Fundam. Appl.* **2019**, *36*, 100723. [CrossRef]
32. Kushwaha, R.K.; Karuppanan, P.; Malviya, L. Design and analysis of novel microstrip patch antenna on photonic crystal in THz. *Phys. B Condens. Matter* **2018**, *545*, 107–112. [CrossRef]
33. Younssi, M.; Jaoujal, A.; Yaccoub, M.D.; El Moussaoui, A.; Aknin, N. Study of a Microstrip Antenna with and Without Superstrate for Terahertz Frequency. *Int. J. Innov. Appl. Stud.* **2013**, *2*, 369–371.
34. Jha, K.R.; Singh, G. Dual-band rectangular microstrip patch antenna at terahertz frequency for surveillance system. *J. Comput. Electron.* **2010**, *9*, 31–41. [CrossRef]
35. Krishna, C.M.; Das, S.; Nella, A.; Lakrit, S.; Madhav, B.T.P. A Micro-Sized Rhombus-Shaped THz Antenna for High-Speed Short-Range Wireless Communication Applications. *Plasmonics* **2021**, *16*, 2167–2177. [CrossRef]
36. Sharma, A.; Dwivedi, V.K.; Singh, G. THz rectangular microstrip patch antenna on multilayered substrate for advance wireless communication systems. In Proceedings of the Progress in Electromagnetics Research Symposium, Beijing, China, 23–27 March 2009; Volume 1, pp. 617–621.
37. Johansson, J.; Whyborn, N. The diagonal horn as a sub-millimeter wave antenna. *IEEE Trans. Microw. Theory Tech.* **1992**, *40*, 795–800. [CrossRef]
38. Chattopadhyay, G.; Alonso-Delpino, M.; Chahat, N.; González-Ovejero, D.; Lee, C.; Reck, T. Terahertz Antennas and Feeds. In *Aperture Antennas for Millimeter and Sub-Millimeter Wave Applications*; Signals and Communication Technology; Springer: Cham, Switzerland, 2018; pp. 335–386. [CrossRef]
39. Reck, T.J.; Jung-Kubiak, C.; Gill, J.; Chattopadhyay, G. Measurement of Silicon Micromachined Waveguide Components at 500–750 GHz. *IEEE Trans. Terahertz Sci. Technol.* **2013**, *4*, 33–38. [CrossRef]
40. Krishna, C.M.; Das, S.; Lakrit, S.; Lavadiya, S.; Madhav, B.T.P.; Sorathiya, V. Design and analysis of a super wideband (0.09–30.14 THz) graphene based log periodic dipole array antenna for terahertz applications. *Optik* **2021**, *247*, 167991. [CrossRef]